Palaeogeography, Palaeoclimatology, Palaeoecology 433 (2015) 1–9

Contents lists available at ScienceDirect

Palaeogeography, Palaeoclimatology, Palaeoecology

journal homepage: www.elsevier.com/locate/palaeo

Sedimentary records of past earthquakes in Boraboy Lake during the last ca 600 years (North Anatolian Fault, Turkey)

Ulaş Avşar [a,b,*], Aurélia Hubert-Ferrari [c], Marc De Batist [a], Sabine Schmidt [d], Nathalie Fagel [e]

[a] Renard Centre of Marine Geology (RCMG), Ghent University, Krijgslaan 281, 9000 Gent, Belgium
[b] Division of Physical Sciences and Engineering, King Abdullah University of Science and Technology (KAUST), 23955-6900 Thuwal, Kingdom of Saudi Arabia
[c] Unit of Physical and Quaternary Geography, University of Liège, Sart Tilman, B-4000 Liège, Belgium
[d] UMR 5805 EPOC OASU, University of Bordeaux, 33615 Pessac, France
[e] AGEs, Department of Geology, University of Liège, Sart Tilman, B-4000 Liège, Belgium

ARTICLE INFO

Article history:
Received 4 January 2015
Received in revised form 27 April 2015
Accepted 29 April 2015
Available online 21 May 2015

Keywords:
Boraboy Lake
Lacustrine paleoseismology
Radiochronology
Seismoturbidite
Homogenite
Mass-wasting deposits

ABSTRACT

Multiproxy sedimentological analyses along 4.9 m-long sequence of Boraboy Lake, which is located on the central eastern part of the North Anatolian Fault (NAF), reveal the sedimentary traces of past large earthquakes in the region. The lake has a relatively large catchment area (10 km^2) compared to its size (0.12 km^2), which renders sedimentation sensitive to heavy rain/storm events. Accordingly, the background sedimentation, which is composed of faintly laminated reddish/yellowish brown clayey silt, is frequently interrupted by organic-rich intercalations probably due to heavy rain/storm events transporting terrestrial plant remains from the densely vegetated catchment. In addition to frequent organic-rich intercalations, the background sedimentation is interrupted by four mass-wasting deposits (MWD) of which thickness range is between 15 and 50 cm. High-resolution ITRAX μXRF data confirms higher homogeneity along the MWDs (E1–E4) compared to the background sedimentation. Based on ^{137}Cs and $^{210}Pb_{xs}$ dating and radiocarbon chronology, three MWDs detected in Boraboy sequence (E2, E3 and E4) temporally correlate with large historical earthquakes along the NAF; the 1943 Tosya ($M_s = 7.6$) and/or 1942 Niksar-Erbaa ($M_s = 7.1$), the 1776 Amasya-Merzifon and the 1668 North Anatolian ($M_s = 7.9$) earthquakes. The youngest MWD in the sequence (E1), which is dated to early 2000s, does not correlate with any strong earthquake in the region. This MWD was probably a single mass-wasting event due to routine overloading and oversteepening on the delta front formed by the main inlet of the lake. In subaqueous paleoseismology, coevality of multi-location mass-wasting events is used as a criterion to assign a seismic triggering mechanism, and to rule out mass-wasting events due to routine overloading/oversteepening of subaqueous slopes. Within this context, Boraboy sequence provides a valuable example to discuss sedimentological imprints of single- vs. multi-source MWDs.

1. Introduction

In addition to the most commonly applied technique in paleoseismology, i.e. paleoseismic trenching, geological fingerprints of past earthquakes can be found by applying subaqueous paleoseismological techniques on marine and lacustrine sedimentary sequences. The most commonly observed sedimentary traces of past earthquakes are mass-wasting deposits (MWD). Cyclic loading during earthquakes decreases effective stress in the sediments, which results in instabilities on the steep subaqueous basin slopes. The wasted material can be transported to the middle parts of the basin by slumping, debris flows and turbidity currents, and archived in the sedimentary sequence as slump or debris-flow deposits, seismoturbidites and/or homogenites. After the first introduction of the term "homogenite" by Sturm et al. (1995), numerous studies have successfully used homogenites to reveal paleoseismic information (e.g., Chapron et al., 1999; Karlin et al., 2004; Monecke et al., 2006; Beck et al., 2007; Schnellmann et al., 2006; Guyard et al., 2007; Bertrand et al., 2008; Carrillo et al., 2008; Beck, 2009; Waldmann et al., 2011; Campos et al., 2013; Howarth et al., 2014; McHugh et al., 2014; Moernaut et al., 2007, 2014). Another commonly observed consequence of cyclic loading on sediments are in-situ soft-sediment-deformations. Cyclic loading may result in microfaults (e.g., Seilacher, 1969; Monecke et al., 2004, 2006; Beck, 2009; Kagan et al., 2011), microfolds (e.g., Monecke et al., 2004; Kagan et al., 2011), loadcast/pseudonodule/ball-and-pillow structures (e.g., Sims, 1973; Hibsch et al., 1997; Migowski et al., 2004; Monecke et al., 2004; Moretti and Sabato, 2007; Sims, 2012) and liquefaction/fluidization/fluid-escape structures (e.g., Lignier et al.,

* Corresponding author at: Division of Physical Sciences and Engineering, King Abdullah University of Science and Technology (KAUST), 23955-6900 Thuwal, Kingdom of Saudi Arabia. Tel.: +966 2 8080351.
E-mail address: avsarulas@yahoo.com (U. Avşar).

http://dx.doi.org/10.1016/j.palaeo.2015.04.031
0031-0182/

1998; Chapron et al., 2004; Moernaut et al., 2007, 2009; Beck, 2009; Kagan et al., 2011). Moreover, seismically-induced water oscillations (i.e., seiche) may cause in-situ sediment resuspension and redeposition (e.g., Siegenthaler et al., 1987; Doig, 1990, 1991, 1998a,b), or transportation of material from lake shores (e.g., Avşar et al., 2014b). In addition to subaqueous mass-wasting, earthquakes may trigger landslides in lake catchments, which may enhance sediment flux into lakes and leave sedimentary traces in the sequence (e.g., Leroy et al., 2009; Hubert-Ferrari et al., 2012; Avşar et al., 2014a; Howarth et al., 2012, 2014). In addition to seismic shaking, surface faulting during earthquakes may also affect sedimentation, especially in shallow water environments (e.g., Mirecki, 1996; Leroy et al., 2009, 2010; Vologina et al., 2010; Bertrand et al., 2011). For example, tectonic subsidence in shallow basins may result in deepening of the lake and inundation of surrounding land, which may leave traces in the sedimentary sequence.

The sedimentary structures and changes in sedimentation mentioned above are, however, not always of seismic origin. For example, lake water level fluctuations or enhanced sediment influx can be simply due to changes in hydrometeorological conditions, or mass-wasting events can be caused by routine overloading/oversteepening of subaqueous slopes. Some soft-sediment-deformations can even be induced during coring. In order to rule out these possibilities, subaqueous paleoseismology basically seeks for coevality of multi-location mass-wasting events and soft-sediment deformations, and for temporal correlation between observed sedimentary events and historical seismicity records, if available. In this study, we present observations on mass-wasting deposits (MWD) within the sedimentary sequence of Boraboy Lake, which is located on the North Anatolian Fault (NAF), Turkey. The region has well-acknowledged historical seismicity records (e.g., Ambraseys, 2009), which allows evaluating triggering mechanisms of the mass-wasting events. In addition to the seismically-triggered MWDs, the presence of a very recent non-seismically-triggered MWD in the Boraboy sequence allows comparisons to be made of sedimentological imprints of single- versus multi-source MWDs. We will also compare the Boraboy record with the record of Göllüköy Lake, which is another lacustrine paleoseismic record located ca 120 km to the east along the NAF (Avşar et al., 2014b) in order to improve our knowledge on the locations of the historical earthquakes in the region during the last 600 years.

2. The study area

Boraboy Lake (40.8038° N, 36.1535° E, 1062 m a.s.l.) is located at the central eastern part of the NAF, which is a major 1000 km-long dextral strike-slip fault in Turkey (Fig. 1a). It is a small (0.124 km^2) landslide-dammed lake with a maximum water depth of 11 m, and it is located at 7 km from the NAF (Fig. 1b and c). The catchment of the lake is composed of highly weathered Lower – Middle Jurassic age alternations of tuff, shale, greywacke and sandstone units (Herece and Akay, 2003). The inlet of the lake, which is fed by a densely vegetated and relatively big catchment (10.02 km^2), forms a delta at its western shores. The slope angles at the northern and southern margins of the lake basin, as well as at the delta front, reach up to 16° to 20°, which makes them highly susceptible to subaqueous slope failures during an earthquake. In addition, the origin of the lake, i.e. being a landslide-dammed lake, supports the idea that the morphology in and around the lake is highly susceptible to earthquake-triggered landslides. This segment of the NAF was ruptured by the 1943 Tosya Earthquake (Ms = 7.6), which created surface rupture extending 280 km along the NAF. The segment to the east of this one was also ruptured by the 1942 Niksar-Erbaa earthquake (Ms = 7.1), of which surface rupture stopped ca. 40 km to the east of the lake (Barka, 1996). In addition to these instrumentally recorded earthquakes, the region was also affected by the great 1668 North Anatolian Earthquake (Ms = 7.9), of which surface rupture was detected in a paleoseismic trenching site ca 8 km to the NNW of the lake (Ambraseys, 2009; Fraser et al., 2009).

3. Methods

After collection of bathymetric data by using a sonar equipped Garmin GPS Map 178, one gravity (BR2007-G, 78 cm) and one piston core (BR2007-01, 470 cm) were taken from the central and the deepest (~11.0 m) part of the lake in 2007 (Fig. 1c). High-resolution sediment core logging and scanning were done by using a Geotek multi-sensor core logger (MSCL), an ITRAX μXRF core scanner and a SCOPIX X-ray image-processing system. The magnetic susceptibility profiles were obtained at 2 mm increments by the Geotek MSCL at the Institute for Applied Geophysics and Geothermal Energy at the RWTH Aachen University. ITRAX μXRF core scanning was done at the Department of Geology and Geochemistry of Stockholm University, with a resolution

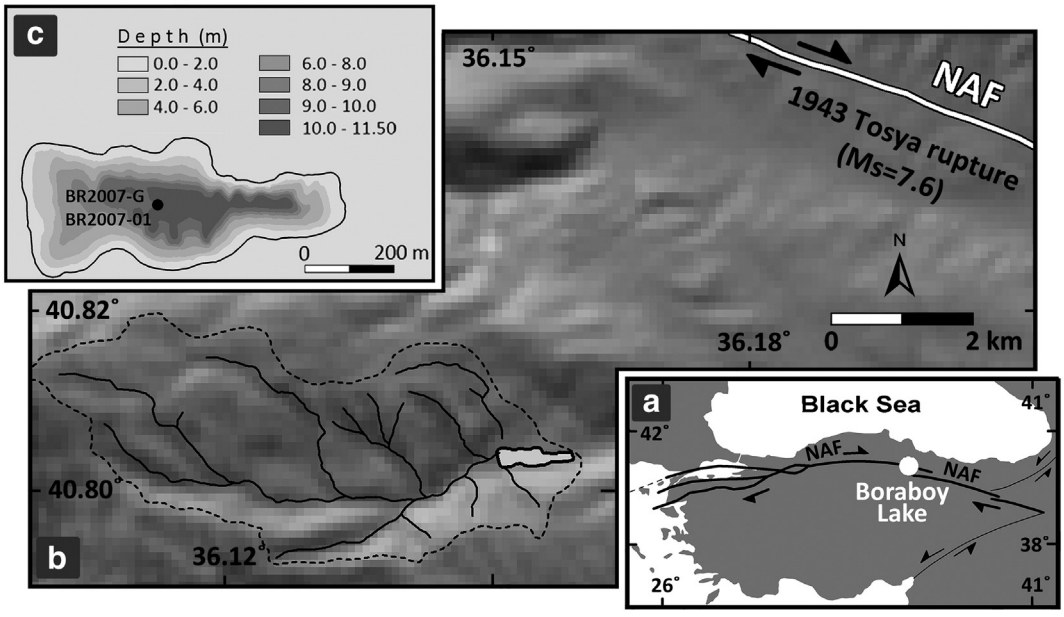

Fig. 1. (a) The geographical setting of the North Anatolian Fault (NAF) and Boraboy Lake. (b) The relief-shaded map illustrating the topography around Boraboy Lake and its catchment, which is located ca 7 km apart from the 1943 Tosya Earthquake (Ms = 7.6) surface rupture. (c) Bathymetric map of the lake and coring location.

of 2 mm and 12 s exposure time with Mo-tube. The radiographic scanning of the BR2007-01 piston core was done on centimeter-thick slabs by the SCOPIX X-ray image-processing system at the EPOC laboratories of University of Bordeaux-I (Migeon et al., 1999). Organic matter content of the sediments was measured at 1 cm increments by the method of weight loss on ignition (LOI) at 550 °C for 4 h (Dean, 1974) at the U. R. Argiles, Géochimie et Environnements sédimentaires (AGEs) of the University of Liège. The activities of ^{137}Cs and excess ^{210}Pb ($^{210}Pb_{xs}$) were measured on 1 cm-thick sediment slices from 18 levels along BR2007-G. The measurements were done by using a low-background, high efficiency well-type gamma spectrometer at the University of Bordeaux (Schmidt et al., 2014). The sediment chronology along the BR2007-01 piston core was established by AMS radiocarbon measurements on terrestrial plant remains. The measurements were done at the AMS facility at the University of Arizona, and the dates were calibrated by using OxCal 4.2.3 software (Bronk Ramsey, 2013) based on the IntCal13 atmospheric curve of Reimer et al. (2013).

4. Background sediments versus event deposits

The optical and radiographic images, magnetic susceptibility, organic matter content (LOI_{550}) and ITRAX μXRF scanning results along the gravity (BR2007-G) and piston (BR2007-01) cores of Boraboy Lake are presented in Fig. 2. The top part of the piston core can be easily

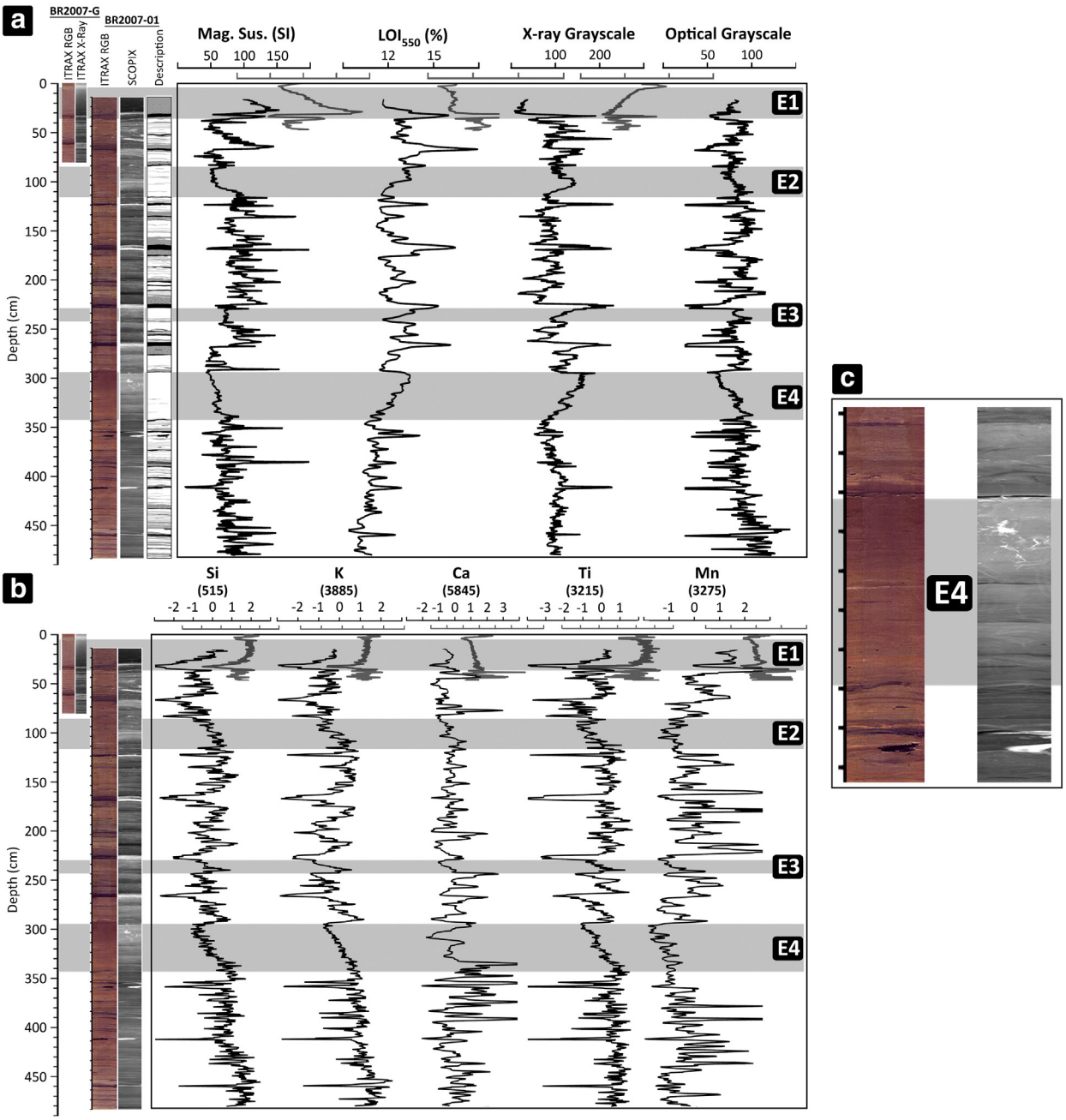

Fig. 2. (a) The optical/radiographic images, magnetic susceptibility, organic matter content (LOI_{550}) and the grayscale plots of the images of Boraboy cores. (b) The results of ITRAX μXRF scanning. The elemental profiles are presented in standardized form and the mean (cps) values for each profile are provided as well. Note that the results for BR2007-G are presented as grey plots having the same scales with the plots of BR2007-01. In the description column of BR2007-01, the coarse- and fine-grained organic matter intercalations (storm and/or heavy rain events) are shown as black and grey layers, respectively. The rest of the description column (white) is reddish/yellowish brown clayey silt. Deposits that are relatively homogenous compared to the background sedimentation are labeled as horizontal grey bars, i.e., E1–E4. (c) A close-up view of E4.

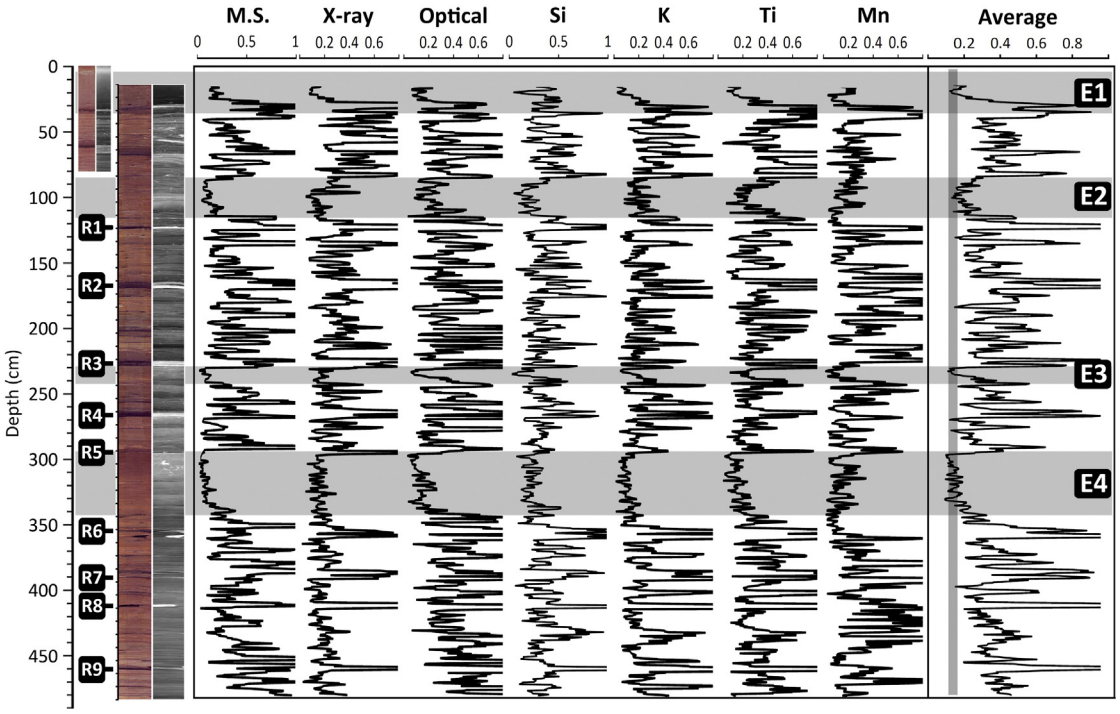

Fig. 3. The plots of standard deviation values obtained by moving a 2 cm-thick window along the measured proxies of the BR2007-01 piston core, and the average of all plots. Along the average plot, note that the homogenous units have lower standard deviation values compared to the background sedimentation. The depths of radiocarbon samples are also shown next to the core image (R1–R9).

correlated with the gravity core, revealing that the top ca. 20 cm of the piston core was lost during coring. The sedimentation in Boraboy Lake is mainly represented by faintly laminated reddish/yellowish brown clayey silt deposition, which is frequently interrupted by organic-rich intercalations and occasionally by relatively homogenous deposits.

Organic-rich intercalations, which are composed of macrofossils of terrestrial plants (mainly leaves), are characterized by relatively darker colors in the optical images, lighter colors in radiographic images, lower magnetic susceptibility values and higher LOI_{550} values (Fig. 2a). Along the ITRAX elemental profiles (Fig. 2b), organic-rich layers tend to have lower counts-per-second values, probably due to the dilution effect of organic matter on X-ray fluorescence. Given their high frequency recurrence and terrestrial origin, we interpret these organic-rich intercalations as the sedimentary traces of storm and/or heavy rain events.

The sequence also contains several relatively homogenous units (E1–E4 in Fig. 2), which are not interrupted by storm and/or heavy rain events. Most of the proxies do not show any significant variations along these deposits. As it is most clearly seen along E4, they are characterized by decreasing upward magnetic susceptibility and optical image grayscale values, and by increasing upward LOI_{550} and radiographic image grayscale values (Fig. 2a). Among the ITRAX μXRF elemental profiles, Si, K and Ti show decreasing upward trends, where Ca and Mn do not show any obvious trends (Fig. 2b). A close-up view of E4 is also provided in Fig. 2c. Fig. 3 presents the plots of standard deviation values of a 2 cm-thick window along the measured proxies, and the average of the plots. Along the average plot, with a few exceptions, the homogenous units have lower standard deviation values compared to the background sedimentation. Another observation is that diatoms, which are typically observed in the background sedimentation, are lacking in these homogenous units (Fig. 4). We interpret the gradual decreasing/increasing upward trends along these deposits as an indication that they were redeposited under the effect of gravitational segregation. For example, the clastic fraction having higher density settles first while the organic fraction is still in suspension, which results in increasing upward LOI_{550} values. In addition, the absence of diatoms in these sediments implies instantaneous deposition. Given these observations, we attribute the homogenous deposits (i.e., turbidites/homogenites) along the sequence (E1–E4) to mass-wasting events, which might

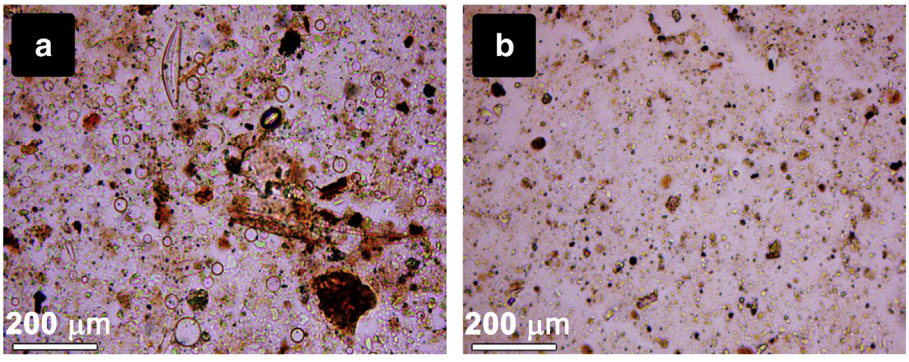

Fig. 4. Representative smear slide images of Boraboy Lake sediments. While the background sedimentation contains diatom population (a), the homogenous units (E1–E4) are almost lack of diatoms (b).

have been triggered by storm and/or heavy rain events, earthquakes, drastic lake level fluctuations or simply over-steepening of the lake basin slopes over time. We investigated the possible seismic origin of these mass-wasting events by establishing a detailed sediment chronology in order to check their temporal correlation with known historical earthquakes in the region.

5. Sediment chronology and age of event deposits

The ^{137}Cs and $^{210}Pb_{xs}$ activity profiles along the BR2007-G core are presented in Fig. 5a. The $^{210}Pb_{xs}$ activity at 3.5 cm depth is significantly lower than the overlying sediments, implying that E1 (3–36 cm) is composed of reworked sediments. In order to determine the background sedimentation rate, the sediments from 3 to 36 cm (i.e. E1) and 56 to 62 cm (i.e. storm/heavy rain deposits) depths should be excluded from the sequence, and the ^{137}Cs and $^{210}Pb_{xs}$ profiles should be re-plotted as a composite sequence (e.g., Arnaud et al., 2002; Schwab et al., 2009). In the composite sequence (Fig. 5b), the main ^{137}Cs peaks in 1986 and 1963 correspond to ca. 19 and 32 cm depths, respectively. Accordingly, along with assuming the top of the core as 2007, the reference points along the ^{137}Cs activity profile yield a background sedimentation rate (SR) of 0.70 cm/yr. The exponential fit on the $^{210}Pb_{xs}$ data presented in Fig. 5b has correlation coefficient of 0.89. The data points at 4.5, 6.5 and 24.5 cm depths (blank circles in Fig. 5b) are not included into the exponential fit because of their high discrepancy from the general trend. The ones at 4.5 and 6.5 cm depths are probably due to a non-distinct storm and/or heavy rain deposits, while the one at 24.5 cm may be related to sediment focusing. Accordingly, the exponential decay of $^{210}Pb_{xs}$ activity results in an SR of 1.04 cm/yr, if "Constant Flux Constant Sedimentation Rate (CFCS)" is assumed. Considering both sedimentation rates from ^{137}Cs and $^{210}Pb_{xs}$ results, E1 is dated to early 2000s and it is not related to any strong earthquake in the region.

For the older mass-wasting events (E2–E4) along the sequence, the sediment chronology is established by radiocarbon dating of ten samples of tree leaves at various depths along the piston core (R0–R9 in Fig. 3). The depths of the samples and the mass-wasting deposits in the bulk and composite sequence, and the obtained radiocarbon dates are presented in Table 1. During the construction of the composite sequence, the storm and/or heavy rain deposits were assumed to be the part of the background sedimentation due to their high frequency of recurrence, and they were not excluded from the sequence; while the homogenous units (E1–E4) were excluded.

In Fig. 6, the calibrated radiocarbon dates, modeled dates of the mass-wasting events and corresponding age–depth models are presented for both bulk (a) and composite (b) sequences. The grey curves along the x axes are the distributions for the single calibrated dates. Although the single calibrated ages have wide ranges of distributions, due to the plateaus in the calibration curve, the sample "R8" at 412 cm depth in the bulk sequence constrains the age as ca. 1460–1660 AD, which results in 0.76–1.17 cm/yr sedimentation rate (SR). In the composite sequence (Fig. 6b), the distribution of "R8" yields an SR of 0.53–0.82 cm/yr, which is slightly lower than the SR calculated by the ^{137}Cs and $^{210}Pb_{xs}$ profiles (i.e., 0.70–1.04 cm/yr). This is reasonable because the deeper parts of the sequence are expected to have lower sedimentation rates due to compaction. In order to better constrain the dates of the MWDs, the modeled ages were calculated by OxCal v4.2.3 (Bronk Ramsey, 2013) based on the "*P_Sequence*" depositional model, which allows random variation from an approximately constant sedimentation rate (Bronk Ramsey, 2008). Accordingly, the marginal posterior distributions for the single modeled ages with 95% confidence interval are shown as black-filled curves, and the age–depth models are presented based on the 68% confidence interval of the modeled ages (the grey polygons down-core). As might be expected, excluding MWDs from the sequence improves the age–depth model, which supports the assumption of instantaneous deposition of E1–E4 (Fig. 6b).

E1 is dated to early 2000s and it does not temporally correlate with any strong earthquake in the region. Within the time span covered by the Boraboy sequence in this study, the best-known NAF earthquakes in the region are the 1943 Tosya Earthquake (Ms = 7.6), the 1942 Niksar-Erbaa Earthquake (Ms = 7.1) and the 1668 North Anatolian Earthquake (Ms = 7.9). E2 is dated to AD 1925–1820 based on

Table 1
Radiocarbon dating results. The depths/intervals of the samples and the mass-wasting event deposits are provided both for the bulk and the composite sedimentary sequences.

	Depth in he sequence	Depth in the composite sequence	Lab number	$F^{14}C$	^{14}C (yr. BP)
R0	67	34	Aeon-27	1.2522 ± 0.0141	Post bomb
R1	122	58	Aeon-28	0.9969 ± 0.0103	25 ± 80
R2	167	103	Aeon-31	0.9955 ± 0.0160	40 ± 130
R3	227	163	Aeon-32	0.9884 ± 0.0057	90 ± 50
R4	266	189	Aeon-33	0.9853 ± 0.0089	120 ± 70
R5	293	216	Aeon-34	0.9668 ± 0.0094	270 ± 80
R6	354	229	Aeon-35	0.9576 ± 0.0108	350 ± 90
R7	391	266	Aeon-36	0.9698 ± 0.0109	250 ± 90
R8	412	287	Aeon-37	0.9638 ± 0.0055	300 ± 50
R9	460	335	Aeon-38	0.9674 ± 0.0111	270 ± 90
E1	3–36	3			
E2	85–116	52			
E3	229–242	165			
E4	294–342	217			

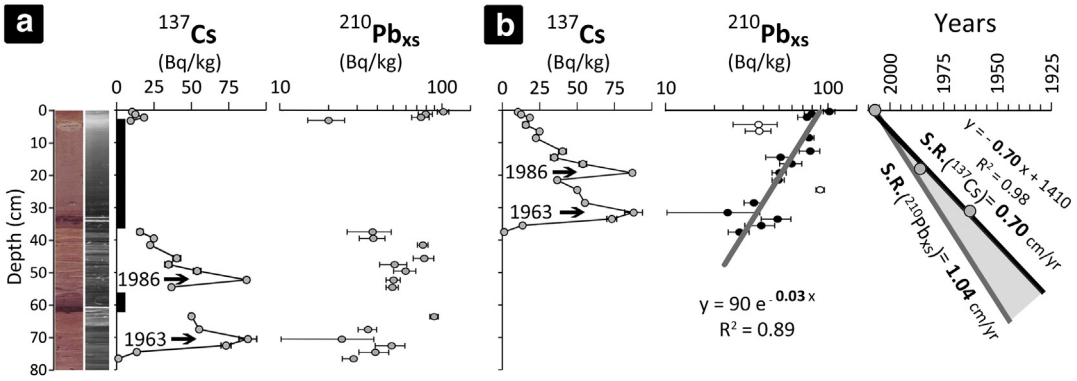

Fig. 5. The results of the ^{137}Cs and $^{210}Pb_{xs}$ measurements along the BR2007-G core, and the calculated mean sedimentation rates (SR). (a) The plots of the results along the bulk sedimentary sequence, and (b) along the composite sequence after excluding instantaneous deposits, i.e., E1 and a storm and/or heavy rain event from 56 to 62 cm depths. The grey line in the rightmost plot in (b) stands for 1.04 cm/yr SR calculated from $^{210}Pb_{xs}$ decay curve, while the black line for 0.70 cm/yr calculated by the reference points along the ^{137}Cs profile.

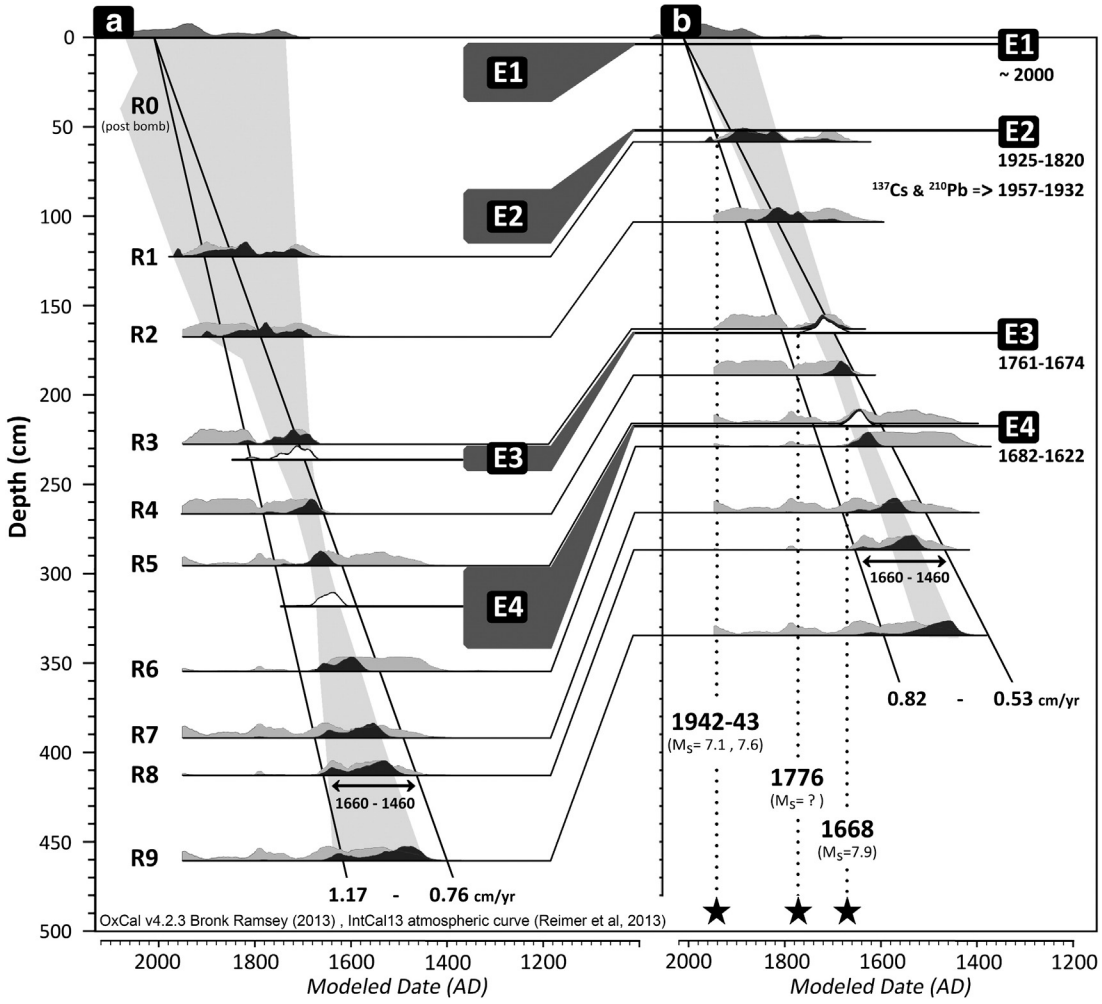

Fig. 6. The radiocarbon chronology for the bulk (a) and composite (b) sedimentary sequences of Boraboy Lake, obtained by using OxCal v4.2.3 software (Bronk Ramsey, 2013), IntCal13 calibration curve of Reimer et al. (2013) and "*P_Sequence*" depositional model of (Bronk Ramsey, 2008). The distributions for the single calibrated dates with 95% confidence interval are plotted along the x axis as grey-filled curves. The overlaying black-filled curves are the marginal posterior distributions for the single modeled dates with 95% confidence interval. The white-filled curves are the distributions of the modeled dates of the MWDs. The age–depth models (grey polygons down-core) are based on the 68% confidence intervals of the modeled dates. Accordingly, E2, E3 and E4 temporally correlate with the well-known earthquakes in the region; i.e., 1943 ($M_s = 7.6$), 1942 ($M_s = 7.1$), 1776 and 1668 ($M_s = 7.9$) earthquakes.

radiocarbon chronology, and to AD 1957–1932 based on the ^{137}Cs and $^{210}Pb_{xs}$ dating (Fig. 6b). Most probably, it was triggered by the 1943 Tosya and/or the 1942 Niksar-Erbaa earthquakes. The oldest event (E4) in the sequence, which is dated to AD 1682–1622, was probably triggered by the giant North Anatolian Earthquake (Ms = 7.9) in AD 1668. This earthquake was the most catastrophic historical earthquake in Anatolia, of which damage zone extended ca. 650 km along the NAF from Bolu-Gerede to Erzincan-Refahiye (Ambraseys, 2009). Probably, that is why E4 is the thickest and the most obvious event along the Boraboy sequence recovered in this study. E3, which is the most non-distinct event in the sequence, is dated to AD 1761–1674 with 95% confidence interval. Historical records report an earthquake in 1776 causing damage in the towns around Boraboy Lake.

Based on the constructed chronology, it is obvious that earthquakes trigger subaqueous slope failures in Boraboy Lake. In addition to MWDs, sedimentary traces of increased sediment influx due to earthquake-triggered landslides in the catchment (i.e., catchment response) can be expected in Boraboy sequence, because the lake has a relatively big catchment. According to the compilation made by Avşar et al. (2014a), the median value of the ratio of catchment area to lake area (CA/LA) of 52 lakes in the lacustrine paleoseismology literature is around 14. They report clear traces of catchment response in Yeniçağa Lake, of which CA/LA is 74, as denser siliciclastic-enriched layers in the sequence. The CA/LA ratio of Boraboy Lake is 81, as high as the ratio of Yeniçağa Lake. However, no clear implications of catchment response are observed in Boraboy Lake. Avşar et al. (2014a) illustrate that the sedimentary traces of catchment response are nondistinct in Yeniçağa Lake during the episodes of high biogenic production in the region, i.e. episodes when the catchment is densely vegetated, which decreases erosion rate. Probably, the traces of catchment response are not clearly observed in Boraboy Lake due to its densely vegetated catchment.

6. Regional paleoseismicity

In order to better understand the paleoseismicity of the NAF in the region, we compared the earthquake sedimentary record Boraboy Lake with the regional historical earthquakes, and also with the lacustrine paleoseismic record of Göllüköy Lake, which is located ca.120 km to the ESE of Boraboy Lake (Fig. 7, modified from Avşar et al. (2014b)). The 20th century earthquakes and the 1668 North Anatolian Earthquake are recorded in both Boraboy and Göllüköy lakes, which are already known as characteristic surface rupturing large earthquakes of the NAF. The earthquakes, which are recorded only in one of the lakes

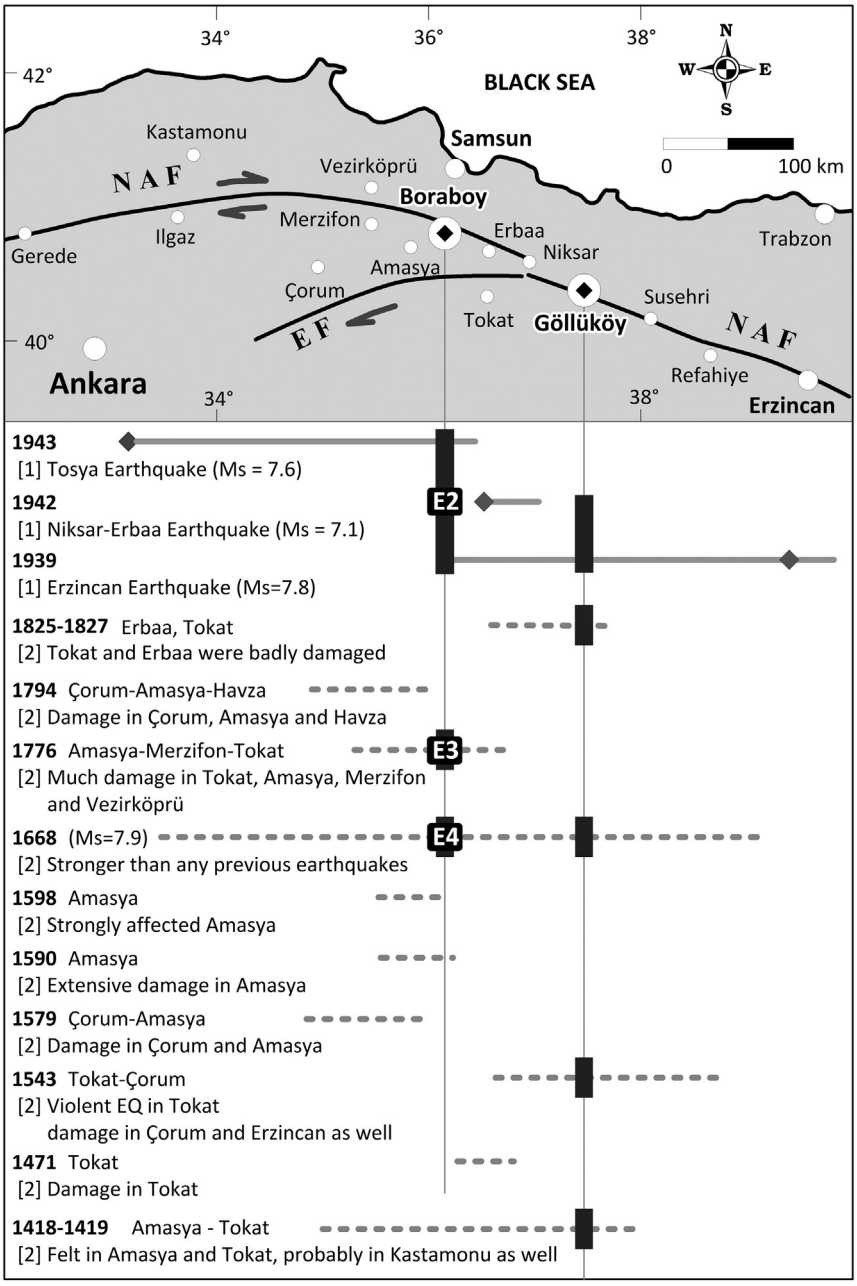

Fig. 7. Comparison of the earthquake sedimentary records from Boraboy (this study) and Göllüköy (Avşar et al., 2014b) lakes with the spatiotemporal distribution of earthquakes along the NAF during the last 600 years ([1] Barka, 1996; [2] Ambraseys, 2009). The upper panel shows the geographic setting of the NAF and the towns referred in the historical seismicity records. The lower panel provides the list of earthquakes during instrumental and historical periods. The horizontal lines corresponding to each earthquake represent known surface ruptures (solid lines) and damage areas described in the historical records (dashed lines) along the NAF. Modified from Avşar et al. (2014b).

(i.e., 1825–1827 Erbaa-Tokat, 1776 Amasya-Merzifon-Tokat, and 1543 Tokat-Çorum), were probably relatively local and smaller ones. None of the remaining historical earthquakes were recorded in the lake sequences, implying that they cannot be large characteristic earthquakes of the NAF.

The record of Boraboy Lake extends back to 1450s, and hence we do not know whether the 1418–1419 Amasya-Tokat Earthquake, which is clearly observed in Göllüköy record, was recorded in Boraboy Lake or not. This earthquake is not recorded in any paleoseismological trenches along the NAF (Fraser et al., 2010). Paleoseismic trenching data shows that the NAF ruptured in that region during the 1668 earthquake and before during a period of high NAF seismicity based on historical earthquakes of AD 967 and AD 1035 in the region, and AD 1050 near Gerede, and AD 1043 and AD 1045 near Erzincan (Fraser et al., 2009). Given the wide spacing between paleoseismological trenches, the 1418–1419 earthquake can still be a $M > 6$ earthquake rupturing the NAF, but we cannot preclude that it is a large regional earthquake off the NAF like the $M = 7.2$ 1916 earthquake (Ambraseys, 1997).

7. Seismically- versus non-seismically-triggered event deposits

The Boraboy sequence contains four mass-wasting deposits, three of which (E2-E4) temporally correlate with past earthquakes in the region. Here, it is worth discussing some sedimentological observations, in which E1 differs from the others. First, while the LOI_{550} profiles along the E2–E4 show increasing-upward trends, it is almost constant along

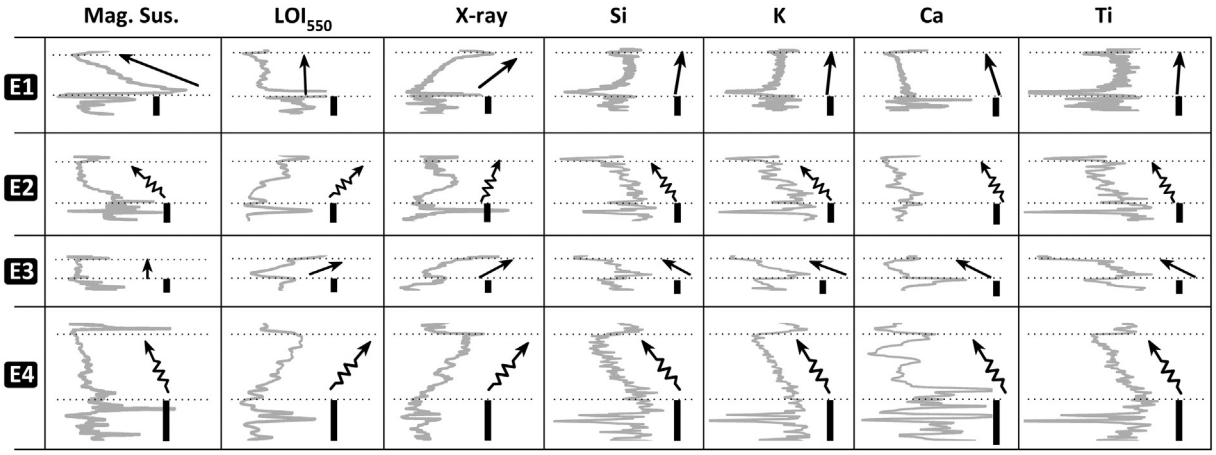

Fig. 8. Comparison of proxies measured along the MWDs in Boraboy sequence. Horizontal dotted lines stand for the upper and lower boundaries of the MWDs. Black rectangles represent approximate values of the measured proxies of the preceding background sediments. Arrowed lines show the general trend of the measured proxies along the MWDs. Zigzags along the arrowed lines imply more heterogeneous nature of earthquake-triggered MWDs compared to E1. E3 is not thick enough to evaluate the homogeneity along it. More heterogeneous nature of E2 and E4 compared to E1 can be attributed to multiple coeval slope failures in the lake due to seismic shock. Note that LOI_{550} profile along E1 has decreasing-upward pattern, while the others have increasing-upward patterns.

E1 (Fig. 8). The trends of LOI_{550} profiles are also confirmed by the μXRF profiles (i.e., Si, K, Ca and Ti), which are indeed affected by organic matter content of sediments. Second, E1 is more homogenous than the other event deposits. Third, E1 has around 2% less organic matter content compared to the preceding background sediments. However, at their lowermost levels, E2–E4 have almost the same organic matter content as the preceding background sediments, and they get more organic-rich towards their upper levels. Based on these observations, we speculate that E1 was a single mass-wasting event, which took place on the delta associated with the main inlet of the lake, while the other event deposits were due to multiple coeval mass-wasting along the slopes of the lake basin. Slight variations of the measured proxies along the E2–E4 deposits may be attributed to multiple sources of sediments, i.e., multi-location coeval mass-wasting events. Moreover, since there are no significant tributaries on the northern and the southern slopes of the lake catchment, the sediments of the delta associated with the main inlet of the lake can be expected to be more dominant in clastics (less organic-rich) than the sediments deposited on the northern and southern basin slopes. This may be the reason why E1 has less organic matter content than the preceding background sediments.

8. Conclusions

In Boraboy Lake, which is a landslide-dammed lake located at ca. 7 km from the NAF, the sedimentary traces of the 1943 Tosya and/or 1942 Niksar-Erbaa (Ms = 7.6 and 7.1, respectively), the 1776 Amasya-Merzifon and the 1668 North Anatolian (Ms = 7.9) earthquakes are found as mass-wasting deposits (MWD). Being the most catastrophic earthquake ever known in Anatolia, the 1668 North Anatolian Earthquake resulted in the thickest MWD within the Boraboy sedimentary sequence recovered in this study. In historical resources, it is sometimes difficult to evaluate which historical earthquakes were large magnitude regional earthquakes. Combining the sedimentary records of Boraboy and Göllüköy lakes, which are ca. 120 km apart from each other, allowed distinguishing between large regional earthquakes and the small local ones. Accordingly, we argue that the historical 1418–1419 Amasya-Tokat Earthquake was a large earthquake in the region like the M = 7.2 1916 earthquake. In addition, the Boraboy sequence allowed a sedimentological comparison to be made between seismically and non-seismically induced MWDs. Basically, seismically-induced MWDs seem more heterogeneous probably due to multi-source sediments transported by coeval multiple mass failures.

Acknowledgments

This research was funded by the European Commission Marie Curie Excellence Grant Project “Understanding the irregularity of seismic cycles: A case study in Turkey” (MEXT-CT-2005-025617: Seismic Cycles), hosted by the Seismology Section of the Royal Observatory of Belgium. The coring was carried out by collaboration with Istanbul Technical University—Eastern Mediterranean Centre for Oceanography and Limnology (ITU-EMCOL). We are grateful to X. Boes, E. Damcı, D. Acar and C. Somuncuoğlu for their assistance and efforts during coring mission.

References

Ambraseys, N.N., 1997. The little-known earthquakes of 1866 and 1916 in Anatolia (Turkey). J. Seismol. 1 (3), 289–299.
Ambraseys, N., 2009. Earthquakes in the Mediterranean and Middle East—A Multidisciplinary Study of Seismicity up to 1900. Cambridge University Press (968 spp.).
Arnaud, F., Lignier, V., Revel, M., Desmet, M., Pourchet, M., Beck, C., Charlet, F., Trentesaux, A., Tribovillard, N., 2002. Flood and earthquake disturbance of ^{210}Pb geochronology (Lake Anterne, North French Alps). Terra Nova 14, 225–232.
Avşar, U., Hubert-Ferrari, A., De Batist, M., Fagel, N., 2014a. A 3400 year lacustrine paleoseismic record from the North Anatolian Fault, Turkey: implications for bimodal recurrence behaviour. Geophys. Res. Lett. 41 (2), 377–384.
Avşar, U., Hubert-Ferrari, A., De Batist, M., Lepoint, G., Schmidt, S., Fagel, N., 2014b. Seismically-triggered organic-rich layers in recent sediments from Göllüköy Lake (North Anatolian Fault, Turkey). Quat. Sci. Rev. 103, 67–80.
Barka, A.A., 1996. Slip distribution along the North Anatolian Fault associated with large earthquakes of the period 1939 to 1967. Bull. Seismol. Soc. Am. 86, 1238–1254.
Beck, C., 2009. Late Quaternary lacustrine paleoseismic archives in north-western Alps: examples of earthquake-origin assessment of sedimentary disturbances. Earth Sci. Rev. 96, 327–344.
Beck, C., Mercier de Lepinay, B., Schneider, J.L., Cremer, M., Çağatay, M.N., Wendenbaum, E., Boutareaud, S., Menot, G., Schmidt, S., Weber, O., Eris, K.K., Armijo, R., Meyer, B., Pondard, N., Gutscher, M.A., MARMARACORE cruise party, 2007. Late Quaternary co-seismic sedimentation in the Sea of Marmara's deep basins. Sediment. Geol. 199, 65–89.
Bertrand, S., Charlet, F., Chapron, E., Fagel, N., De Batist, M., 2008. Reconstruction of the Holocene seismotectonic activity of the Southern Andes from seismites recorded in Lago Icalma, Chile, 39°S. Palaeogeogr. Palaeoclimatol. Palaeoecol. 259, 301–322.
Bertrand, S., Doner, L., Akçer Ön, S., Sancar, U., Schudack, U., Mischke, S., Çagatay, M.N., Leroy, S.A.G., 2011. Sedimentary record of coseismic subsidence in Hersek coastal lagoon (Izmit Bay, Turkey) and the late Holocene activity of the North Anatolian Fault. Geochem. Geophys. Geosyst. 12, Q06002. http://dx.doi.org/10.1029/2011GC003511.
Bronk Ramsey, C., 2008. Deposition models for chronological records. Quat. Sci. Rev. 27, 42–60.
Bronk Ramsey, C., 2013. OxCal Program v. 4.2.3 Radiocarbon Accelerator unit. University of Oxford, Oxford, U.K. (Available at https://c14.arch.ox.ac.uk/oxcal.html).
Campos, C., Beck, C., Crouzet, C., Demory, F., Van Welden, A., Eris, K., 2013. Deciphering hemipelagites from homogenites through anisotropy of magnetic susceptibility. Paleoseismic implications (Sea of Marmara and Gulf of Corinth). Sediment. Geol. 292, 1–14.

Carrillo, E., Beck, C., Audemard, F.A., Moreno, E., Ollarves, R., 2008. Disentangling Late Quaternary climatic and seismo-tectonic controls on Lake Mucubají sedimentation (Mérida Andes, Venezuela). In: De Batist, M., Chapron, E. (Eds.), Lake systems: sedimentary archives of climate change and tectonic. Palaeogeography, Palaeoclimatology, Palaeoecology 259, pp. 284–300.
Chapron, E., Beck, C., Pourchet, M., Deconinck, J.F., 1999. 1822 AD earthquake-triggered homogenite in Lake Le Bourget (NW Alps). Terra Nova 11, 86–92.
Chapron, E., Van Rensbergen, P., De Batist, M., Beck, C., Henriet, J.-P., 2004. Fluid-escape features as a precursor of large sub-lacustrine sediment slide in Lake Le Bourget, NWAlps, France. Terra Nova 16 (5), 305–311.
Dean Jr., W.E., 1974. Determination of carbonate and organic matter in calcareous sediments and sedimentary rocks by loss on ignition: comparison with other methods. J. Sediment. Petrol. 44, 242–248.
Doig, R., 1990. 2300 yr history of seismicity from silting events in Lake Tadoussac, Charlevoix, Quebec. Geology 18, 820–823.
Doig, R., 1991. Effects of strong seismic shaking in lake sediments, and earthquake recurrence interval, Te´miscaming, Quebec. Can. J. Earth Sci. 28, 1349–1352.
Doig, R., 1998a. Paleoseismological evidence from lake sediments for recent movement on the Denali and other faults, Yukon Territory, Canada. Tectonophysics 296, 363–370.
Doig, R., 1998b. 3000-year paleoseismological record from the region of the 1988 Saguenay, Quebec, earthquake. Bull. Seismol. Soc. Am. 88 (5), 1198–1203.
Fraser, J.G., Pigati, J.S., Hubert-Ferrari, A., Vanneste, K., Avsar, U., Altinok, S., 2009. A 3000-year record of ground-rupturing earthquakes along the central North Anatolian Fault near Lake Ladik. Turk. Bull. Seismol. Soc. Am. 99 (5), 2681–2703.
Fraser, J.G., Vanneste, K., Hubert-Ferrari, A., 2010. Recent behavior of the North Anatolian Fault: insights from an integrated paleoseismological data set. J. Geophys. Res. 115, B09316. http://dx.doi.org/10.1029/2009JB006982.
Guyard, A., St-Onge, G., Chapron, E., Anselmetti, F.S., Francus, P., 2007. The AD1881 earthquake triggered slump and late holocene flood-induced Turbidites from Proglacial Lake Bramant, Western French Alps. In: Lykousis, V., Sakellariou, D., Locat, J. (Eds.), Submarine Mass Movements and their Consequences. Springer, Berlin, pp. 279–286.
Herece, E., Akay, E., 2003. Kuzey Anadolu Fayı (KAF) Atlası/Atlas of the North Anatolian Fault (NAF). Maden Tetkik Arama Genel Müdürlüğü Special Publications Ser. 2, Ankara, 61 pp. + 13 appendices as separate maps.
Hibsch, C., Alvarado, A., Yepes, H., Perez, V.H., Sebrier, M., 1997. Holocene liquefaction and soft-sediment deformation in Quito (Ecuador): a paleoseismic history recorded in lacustrine sediments. J. Geodyn. 24, 259–280.
Howarth, J.D., Fitzsimons, S.J., Norris, R.J., Jacobsen, G.E., 2012. Lake sediments record cycles of sediment flux driven by large earthquakes on the Alpine fault, New Zealand. Geology 40 (12), 1091–1094.
Howarth, J.D., Fitzsimons, S.J., Norris, R.J., Jacobsen, G.E., 2014. Lake sediments record high intensity shaking that provides insight into the location and rupture length of large earthquakes on the Alpine Fault, New Zealand. Earth Planet. Sci. Lett. 403, 340–351.
Hubert-Ferrari, A., Avsar, U., El Ouahbi, M., Lepoint, G., Fagel, N., 2012. Paleoseismic record obtained by coring a lacustrine sag-pond along the North Anatolian Fault (Turkey). Ann. Geophys. 55 (5), 929–953.
Kagan, E., Stein, M., Agnon, A., Neumann, F., 2011. Intrabasin paleoearthquake and quiescence correlation of the late Holocene Dead Sea. J. Geophys. Res. 116, B04311. http://dx.doi.org/10.1029/2010JB007452.
Karlin, R.E., Holmes, M., Abella, S.E.B., Sylwester, R., 2004. Holocene landslides and a 3500-year record of Pacific Northwest earthquakes from sediments in Lake Washington. GSA Bull. 116, 94–108.
Leroy, S.A.G., Boyraz, S., Gürbüz, A., 2009. High-resolution palynological analysis in Lake Sapanca as a tool to detect recent earthquakes on the North Anatolian Fault. Quat. Sci. Rev. 28, 2616–2632.
Leroy, S.A.G., Schwab, M.J., Costa, P.J.M., 2010. Seismic influence on the last 1500-year infill history of Lake Sapanca (North Anatolian Fault, NW Turkey). Tectonophysics 486, 15–27.
Lignier, V., Beck, C., Chapron, E., 1998. Caractérisation géométrique et texturale de perturbations synsédimentaires attribuées à des séismes, dans une formation quaternaire glaciolacustre des Alpes (les Argiles du Trièves). C.R. Acad. Sci. Paris. Earth Planet. Sci. 327, 645–652.
McHugh, C.M.G., Braudy, N., Çağatay, M.N., Sorlien, C., Cormier, M.-H., Seeber, L., Henry, P., 2014. Seafloor fault ruptures along the North Anatolia Fault in the Marmara Sea, Turkey: Link with the adjacent basin turbidite record. Mar. Geol. 353 (1), 65–83.
Migeon, S., Weber, O., Faugeres, J., Saint-Paul, J., 1999. SCOPIX: a new X-ray imaging system for core analysis. Geo-Mar. Lett. 18, 251–255.
Migowski, C., Agnon, A., Bookman, R., Negendank, J.F.W., Stein, M., 2004. Recurrence pattern of Holocene earthquakes along the Dead Sea transform revealed by varve-counting and radiocarbon dating of lacustrine sediments. Earth Planet. Sci. Lett. 222, 301–314.
Mirecki, J.E., 1996. Recognition of the 1811–1812 New Madrid earthquakes in Reelfoot Lake, Tennessee sediments using pollen data. J. Paleolimnol. 15, 183–191.
Moernaut, J., De Batist, M., Charlet, F., Heirman, K., Chapron, E., Pino, M., Brümmer, R., Urrutia, R., 2007. Giant earthquakes in South-Central Chile revealed by Holocene mass-wasting events in Lake Puyehue. Sediment. Geol. 195, 239–256.
Moernaut, J., De Batist, M., Heirman, K., Van Daele, M., Pino, M., Brümmer, R., Urrutia, R., 2009. Fluidization of buried mass-wasting deposits in lake sediments and its relevance for paleoseismology: results from a reflection seismic study of lakes Villarrica and Calafquén (South-Central Chile). Sediment. Geol. 213, 121–135.
Moernaut, J., Van Daele, M., Heirman, K., Fontijn, K., Strasser, M., Pino, M., Urrutia, R., De Batist, M., 2014. Lacustrine turbidites as a tool for quantitative earthquake reconstruction: new evidence for a variable rupture mode in South-Central Chile. J. Geophys. Res. http://dx.doi.org/10.1002/2013JB010738.
Monecke, K., Anselmetti, F.S., Becker, A., Sturm, M., Giardini, D., 2004. Signature of historic earthquakes in lake sediments in Central Switzerland. Tectonophysics 394, 21–40.
Monecke, K., Anselmetti, F.S., Becker, A., Schnellmann, M., Sturm, M., Giardini, D., 2006. Earthquake-induced deformation structures in lake deposits: a late Pleistocene to Holocene Paleoseismic record for Central Switzerland. Eclogae Geol. Helv. 99, 343–362.
Moretti, M., Sabato, L., 2007. Recognition of trigger mechanisms for soft-sediment deformation in the Pleistocene lacustrine deposits of the Sant'Arcangelo Basin (southern Italy): seismic shock vs. overloading. Sediment. Geol. 196, 31–45.
Reimer, P.J., et al., 2013. IntCal13 and Marine13 radiocarbon age calibration curves, 0–50,000 years cal BP. Radiocarbon 55 (4), 1869–1887.
Schmidt, S., Howa, H., Diallo, A., Martín, J., Cremer, M., Duros, P., Fontanier, Ch., Deflandre, B., Metzger, E., Mulder, Th., 2014. Recent sediment transport and deposition in the Cap-Ferret Canyon, South-East margin of Bay of Biscay. Deep Sea Res.ss II. http://dx.doi.org/10.1016/j.dsr2.2013.06.004.
Schnellmann, M., Anselmetti, F.S., Giardini, D., McKenzie, J.A., 2006. 15,000 years of mass-movement history in Lake Lucerne: implications for seismic and tsunami hazards. Eclogae Geol. Helv. 99, 409–428.
Schwab, M.J., Werner, P., Dulski, P., McGee, E., Nowaczyk, N.R., Bertrand, S., Leroy, S.A.G., 2009. Palaeolimnology of Lake Sapanca and identification of historic earthquake signals, Northern Anatolian Fault Zone (Turkey). Quat. Sci. Rev. 28 (11–12), 991–1005.
Seilacher, A., 1969. Fault-graded beds interpreted as seismites. Sedimentology 13, 155–159.
Siegenthaler, C., Finger, W., Kelts, K., Wang, S., 1987. Earthquake and seiche deposits in Lake Lucerne, Switzerland. Eclogae Geol. Helv. 80, 241–260.
Sims, J.D., 1973. Earthquake-induced structures in sediments of Van Norman Lake, San Fernando, California. Science 182, 161–163.
Sims, J.D., 2012. Earthquake-induced load casts, pseudonodules, ball-and-pillow structures, and convolute lamination: additional deformation structures for paleoseismic studies. In: Cox, R.T., Tuttle, M.P., Boyd, O.S., Locat, J. (Eds.), Recent Advances in North American Paleoseismology and Neotectonics East of the Rockies: Geological Society of America Special Paper 493, pp. 191–201. http://dx.doi.org/10.1130/2012.2493(09).
Sturm, M., Siegenthaler, C., Pickrill, R.A., 1995. Turbidites and 'homogenites'. A conceptual model of flood and slide deposits. Publication IAS-16th Regional Meeting of Sedimentology, Paris. 22, p. 140.
Vologina, E.G., Kalugin, I.A., Osukhovskaya, Yu.N., Sturm, M., Ignatova, N.V., Radziminovich, Ya.B., Dar'in, A.V., Kuz'min, M.I., 2010. Sedimentation in Proval Bay (Lake Baikal) after earthquake-induced subsidence of part of the Selenga River delta. Russ. Geol. Geophys. 51, 1275–1284.
Waldmann, N., Anselmetti, F.S., Ariztegui, D., Austin Jr., J.A., Pirouz, M., Moyz, C.M., Dunbark, R., 2011. Holocene mass-wasting events in Lago Fagnano, Tierra del Fuego (54°S): implications for paleoseismicity of the Magallanes–Fagnano transform fault. Basin Res. 23, 171–190.